Hydrosilylation of Alkynes Under Continuous Flow Using Polyurethane-Based Monolithic Supports with Tailored Mesoporosity

Hande Acikalin, Pradeep K. R. Panyam, Abdul Wasif Shaikh, Dongren Wang, Shravan R. Kousik, Petia Atanasova, and Michael R. Buchmeiser*

Non-porous polyurethane-based monoliths are prepared under solvent-induced phase separation conditions. They possess low specific surface areas of 0.15 m^2 g^{-1}, pore volumes of 1 µL g^{-1}, and a non-permanent, solvent-induced microporosity with pore dimensions ≤1 nm. Mesoporosity can be introduced by varying the monomers and solvents. A tuning of the average solubility parameter of the solvent mixture by increasing the macroporogen content results in a decrease in the volume fraction of micropores from 70% to 40% and an increase in the volume fraction of pores in the range of 1.7–9.6 nm from 22% to 41% with only minor changes in the volume fraction of larger mesopores in the range of 9.6–50 nm. The polymeric monoliths are functionalized with quaternary ammonium groups, which allowed for the immobilization of an ionic liquid that contained the ionic Rh-catalyst [1-(pyrid-2-yl)-3-mesityl)-imidazol-2-ylidene))(η^4-1,5-cyclooctadiene)Rh(I) tetrafluoroborate]. The supported catalyst is used in the hydrosilylation of 1-alkynes with dimethylphenylsilane under continuous flow using methyl-*tert*-butyl ether as second liquid transport phase. *E/Z*-selectivity in hydrosilylation is compared to the one of the analogous biphasic reactions. The strong increase in *Z*-selectivity is attributed to a confinement effect provided by the small mesopores.

H. Acikalin, P. K. R. Panyam, A. W. Shaikh, D. Wang, M. R. Buchmeiser
Institute of Polymer Chemistry
University of Stuttgart
Pfaffenwaldring 55, D-70569 Stuttgart, Germany
E-mail: michael.buchmeiser@ipoc.uni-stuttgart.de
S. R. Kousik, P. Atanasova
Institute of Materials Science
University of Stuttgart
Heisenbergstraße 3, D-70569 Stuttgart, Germany
M. R. Buchmeiser
German Institutes of Textile and Fiber Research (DITF) Denkendorf
Körschtalstr. 26, D-73770 Denkendorf, Germany
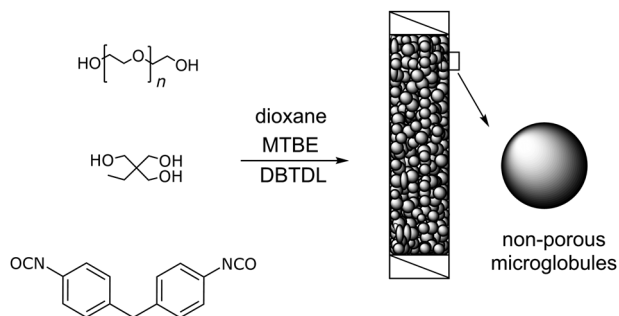
1. Introduction

Polymeric monolithic materials developed some 40 years ago as non-porous separation media ("stationary phases") for the separation of large analytes such as desoxyribonucleic acid (DNA), oligonucleotides, proteins, and peptides.[1–3] Since then, they have become a prominent part of the armor of stationary phases for the separation of bio(macro-)molecules.[4–6] In view of their most appealing characteristics such as high permeability, lack of micro-, meso- and macroporosity and fast mass transfer between the stationary and the mobile phase[7–11] it is not surprising that polymeric monoliths also found increasing application as supports in heterogeneous catalysis under continuous conditions.[12] While the majority of polymeric monolithic media for catalytic purposes have been prepared by ring-opening metathesis polymerization (ROMP) of norbornenes[13,14] or via the free radical polymerization of styrenes,[15–18] the use of polyurethane-based systems is very scarce.[19,20] Within that context, polyurethane/cellulose-based hybrid monoliths have been used in a continuous biphasic supported ionic liquid phase setup in which the enzyme CALB was immobilized in an ionic liquid (IL).[21–23] Compared to poly(norbornene) or poly(styrene) based monoliths, polyurethane-based monoliths are more polar and offer the possibility of surface functionalization via excess hydroxyl or isocyanate groups. In course of our activities in the area of molecular heterogeneous catalysis in confined geometries[24–30] we were interested in synthesizing polyurethane-based monolithic supports that fulfill the general requirements for polymeric monoliths such as unitary structure, incompressibility, transport pores in the micrometer range, high linear flow (up to 20 mm s^{-1}) at low back pressure (<10 bar), while having a tailored mesoporosity in the 2–10 nm range. These mesoporous monoliths were then surface functionalized with quaternary ammonium groups followed by immobilization of an ionic Rh-catalyst-containig IL for use in heterogeneous, biphasic, continuous catalysis using the mesopores as confinements[31–33] that ultimately govern the reactivity of the Rh-catalyst.

**ADVANCED
SCIENCE NEWS**

www.advancedsciencenews.com

[M]acro-molecular
Chemistry and Physics

www.mcp-journal.de

Scheme 1. Synthesis of non-porous polyurethane-based monoliths prepared from PEG$_{300}$, TMP, MDI, DBTDL in a dioxane/MTBE mixture.

2. Results and Discussion

2.1. Synthesis of Monoliths Under Solvent-Induced Phase Separation (SIPS) and Origin of Porosity

Polymeric monolithic materials can be prepared under solvent-induced phase-separation conditions within the confines of choice, for example, a reactor column, using appropriate amounts of monomers, crosslinkers, and a mixture of porogenic solvents.[3,14,34–37] The latter is usually based on both a good and a bad solvent for the corresponding polymer, thereby serving as microporogen and macroporogen, respectively. Within this context, the terms "good" and "bad" polymer solvent refer to solvent/polymer systems that have small and large differences in the solubility (Hildebrand) parameters, δ, respectively.

Generally, the microstructure of polymeric monoliths in terms of porosity and size of the structure-forming microglobules greatly depends on the onset of phase separation, which is affected by both the solvents used and the degree of crosslinking at a given monomer conversion. Also, the process needs to be designed such that phase separation is faster than gelation. According to the Flory–Huggins theory, the entropy term in Equation (1) is always negative, but small. Consequently, the enthalpy term in Equation (1) needs to be largely positive in order to provide a value for ΔG_{mix} that is also positive, a requirement for phase separation to occur. Hence, the Flory–Huggins interaction parameter (X_{12}) between the polymer and the solvent mixture needs to be substantially larger than zero and the monomers, crosslinkers, and solvents have to be chosen accordingly.

$$\Delta G_{mix} = \Delta H_{mix} - T\Delta S_{mix}$$

$$\Delta G_{mix} \sim RT[(\Phi_1/P_1)\ln\Phi_1 + (\Phi_2/P_2)ln\Phi_2 + X_{12}\Phi_1\Phi_2] \quad (1)$$

2.2. Non-Porous Polyurethane-Based Monoliths

In view of these requirements, non-porous polyurethane-based monoliths were prepared under solvent-induced phase separation (SIPS) conditions (**Scheme 1**).

Methylenediphenyl diisocyanate (MDI) polyethylene glycol (PEG$_{300}$), and 1,1,1-tris(hydroxymethyl)propane (TMP) were used as monomers, dibutyltin dilaurate (DBTDL) as catalyst, dioxane and methyl *tert*-butyl ether (MTBE) as solvents. Table 2 summarizes the composition of the reaction mixture. The tailored monomer:crosslinker ratio offered access to non-porous
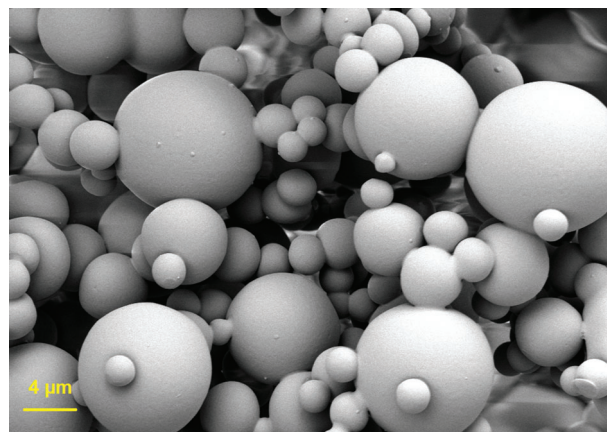

Figure 1. SEM picture of the non-porous poly(urethane)-derived monolith **P1**.

polyurethane monoliths that allowed for high linear flow rates (≤13 mm min^{-1}) at low counter back pressure (6–7 bar). The polyaddition reaction was carried out in a vertically oriented steel column (8 × 300 mm) at 45 °C over 18 h. Once the reaction was complete, columns were flushed with CHCl$_3$ at a flow rate of 2.0 mL min^{-1} for 3 h to remove the catalyst, the solvents, and any unreacted monomer. The typical microstructure of a non-porous polyurethane-based monolith is shown in **Figure 1**.

One can clearly see the structure-forming microglobules 2–12 µm in diameter. The monoliths had a specific surface area (σ) of 0.157 m^2 g^{-1} and a very small pore volume of 1 µL g^{-1} as determined by N$_2$-sorption (**Table 1**). In contrast to nitrogen-sorption measurements (Figure S2, Supporting Information), inverse-size exclusion chromatography (ISEC)[38,39] revealed a high abundance of micropores ≤2 nm reaching 70% of the total pore volume (monolith **P1**, Figure S2, Supporting Information). The volume fraction of the intermicroglobule void volume (interstitial porosity) as determined by ISEC was 67%, which explains the good permeability of the monoliths, resulting in the above-mentioned low back pressures at high linear flow rates. The discrepancy between N$_2$-sorption and ISEC data can be rationalized in light of the different experimental conditions used in these two analytical methods. Thus, N$_2$-sorption is performed in dry conditions while ISEC is performed in the presence of a good polymer solvent that induces swelling of the polymeric monolith (here CHCl$_3$). While drying results in the shrinkage and an almost complete collapse of the micropores, the use of CHCl$_3$ induces a non-permanent swelling microporosity in the range of approximately one nanometer.

2.3. Polyurethane-Based Monoliths with Tailored Mesoporosity

In order to increase the accessible surface area, the SIPS conditions used for the synthesis of non-porous polyurethane monoliths outlined above were modified such that mesoporosity was generated. For these purposes, PEG$_{300}$ was substituted by triethylene glycol (TEG) to increase the polarity of the polymerization mixture, to facilitate mixing of the components, and to allow for larger amounts of the macroporogen. To reduce complexity of the SIPS process, all variations in the polymerization mixture were

**ADVANCED
SCIENCE NEWS**

www.advancedsciencenews.com

Macro-
molecular
Chemistry and Physics

www.mcp-journal.de

Table 1. Recipes for the synthesis of the polyurethane-based monoliths **P1–P5** (all wt.-%); values for the pore volume, V_p, the specific surface area, σ, the volume fraction of pores, ϵ_p, the volume fraction of intermicroglobule void volume (interstitial porosity), ϵ_z, and the total volume fraction, ϵ_t.

#	TMP[a]	PEG$_{300}$	TEG[a]	MDI[a]	DBTDL[a]	MTBE[a]	Dioxane[a]	ϵ_p [%][b]	ϵ_z [%][b]	ϵ_t [%][b]	V_p [mL g^{-1}][b]	σ [m^2 g^{-1}][c]
P1	4.2	1.8		13.1	3.9	53	24	4	63	67	0.62	1.01
P2	4.8		0.08	13.6	2.4	39.6	39.6	6	71	77	0.92	0.69
P3	4.8		0.08	13.6	2.4	43.6	35.6	4	51	55	0.10	0.15
P4	4.8		0.08	13.6	2.4	45.5	33.7	6	50	56	0.12	0.40
P5	5.1		0.08	13.3	2.4	45.5	33.7	4	75	79	0.11	0.50

[a] wt.-%; [b] determined by ISEC; [c] determined by N$_2$-sorption.

restricted to changes in the solvent mixture. The exact composition of the different polymerization mixtures is listed in Table 1. By increasing the amount of MTBE ($\delta = \approx 14.5$ MPa$^{0.5}$) from 39.5 to 45.4 wt.-% on the expense of dioxane ($\delta = 20.3$ MPa$^{0.5}$), whose content was reduced from 39.5 to 33.5 wt.-%, the average Hildebrand solubility parameter decreased, which allowed for shifting the onset of phase separation to an earlier stage of polymerization. This in turn changed the ISEC-derived pore size distribution and resulted in a strong reduction of the volume fraction of micropores (≤ 2 nm) from $\approx 70\%$ to $\approx 40\%$ (Figures S1–S8, Supporting Information). At the same time, the volume fraction of mesopores in the range of 2–10 nm almost doubled (22% → 41%) while the volume fraction of larger mesopores up to 50 nm remained almost constant. The volume fraction of the pores (ϵ_p) and the volume fraction of the inter-microglobule void volume (ϵ_z) were 4–6% and 50–75% respectively (Table 1). These values resulted in a total porosity (ϵ_t) of 55–79%. Considering monolith **P5**, prepared from excess TMP, the large porosity of the monolith still guarantees a low back-pressure under continuous flow, despite the presence of excess hydroxyl groups, which usually lead to a swelling of the support in the presence of polar solvents. Pore volumes (V_p) were in the range of 1–7 µL g^{-1} as determined via N$_2$-sorption analysis compared to 920, 100, 120, and 110 µL g^{-1} for **P2**–**P5** as determined by ISEC, which clearly illustrates the importance of non-permanent (swelling) porosity in these monoliths in "good" polymer solvents such as CHCl$_3$. The drop from 920 to 100–120 µL g^{-1} is in line with a decreased microporosity and an increased mesoporosity in monoliths **P3**–**P5**. Notably, complementary to a recently reported template-based approach,[40] this is the first successful report on a tuning of the pore diameters of monolithic materials in the low mesopore region via SIPS.
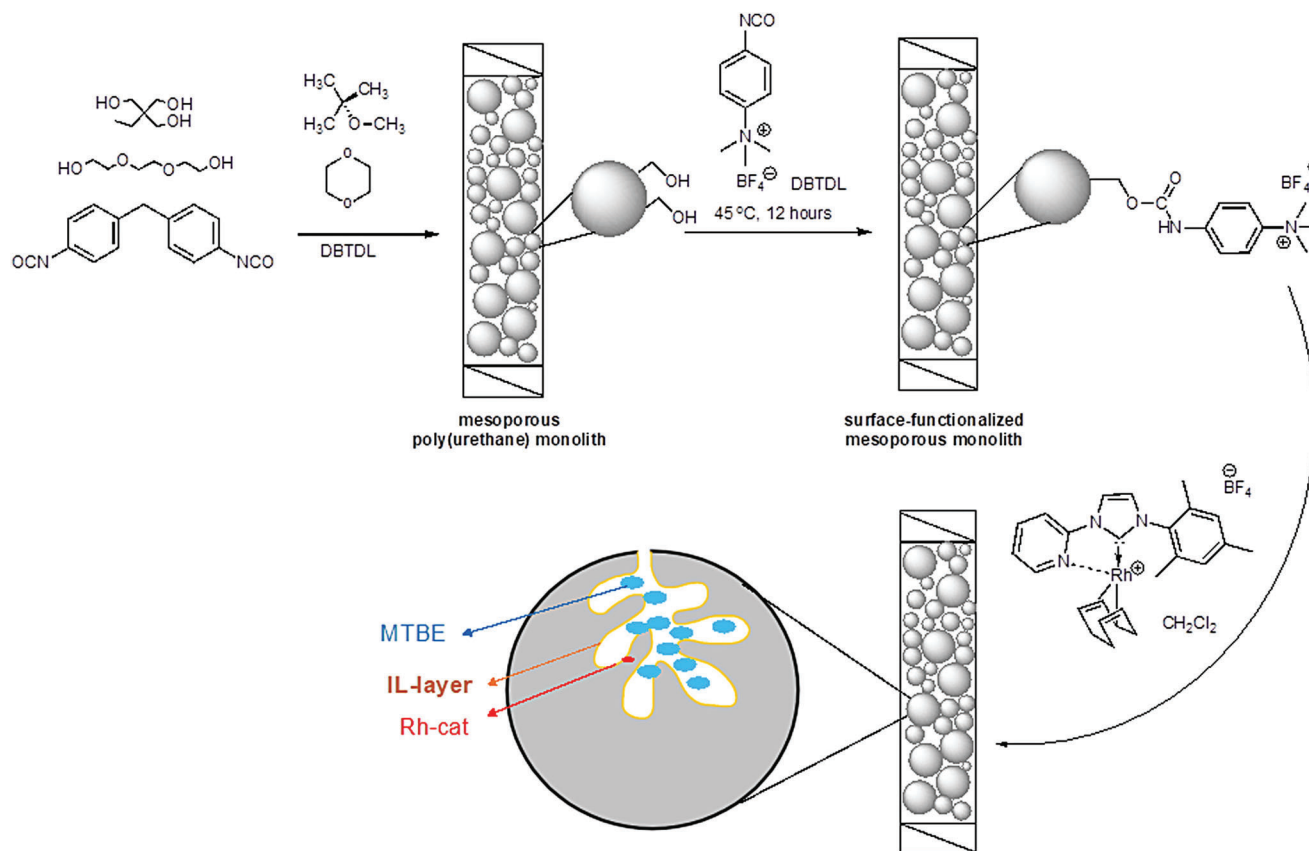
2.4. Surface Functionalization

Monolith **P5** was prepared using a 10% excess of hydroxyl groups with respect to the isocyanate groups (**Scheme 2**). The use of this comparably small excess of hydroxyl groups allowed for keeping the maximum possible conversion of the polyaddition reaction high while still providing $\approx 40\%$ mesoporosity in the range of 2–40 nm. The excess hydroxyl groups were then reacted with [NCO-C$_6$H$_4$-NMe$_3$$^+$][BF$_4$$^-$] in the presence of DBTDL to introduce ionic groups at the monolith's surface, followed by flushing with CH$_2$Cl$_2$ to remove excess [NCO-C$_6$H$_4$-NMe$_3$$^+$][BF$_4$$^-$]. Fi-

nally, the cationic Rh-NHC catalyst and [BMIM$^+$][BF$_4$$^-$] dissolved in CH$_2Cl_2$ were introduced into the monolithic column and vacuum was applied to remove all solvents and to immobilize both the catalyst and the IL on the monolith's surface. Finally, the support was flushed with heptane to remove excess [BMIM$^+$][BF$_4$$^-$].

2.5. Confocal Laser Scanning Microscopy (CLSM) Measurements

In order to determine the distribution and accessibility of excess hydroxyl groups on the monoliths, CLSM investigations were performed with representative fluorescent probe molecules, namely a non-covalent polymeric pore-filling agent (Rhodamine B-PEG, RhB-PEG $M_n = 5000$ g mol^{-1}) and the organosilane 3-(2,4-dinitrophenylamino)propyltriethoxysilane (DPPS), capable of covalently binding to the hydroxyl groups. Monolith **P5** was first treated with RhB-PEG and subsequently functionalized with DPPS. Since RhB-PEG and DPPS fluoresce at different wavelengths, their spatial distributions can be resolved by using different excitation lasers. The CLSM image of a representative optical slice from the middle of the sample is shown in **Figure 2**.

The green and blue regions correspond to the spatial distributions of RhB-PEG and DPPS, respectively. From the CLSM image, it can be seen that RhB-PEG is largely constrained to the surface of the structure-forming microglobules, while DPPS is distributed far more substantively across the porous matrix. A precise visualization of the micropore and mesopore domains was not achieved due to the diffraction-limited resolution of CLSM. However, a qualitative interpretation of the spatial permeation behavior of the two probe molecules can be made on the basis of their molecular size. Since RhB-PEG is much larger than DPPS, its diffusion into the microporous domain is restricted, and thus its localization is constrained to the external surface of the microstructure-forming microglobules. On the other hand, the relatively smaller DPPS is able to permeate into the microporous domain as well. Reference samples in which **P5** was only treated with RhB-PEG and DPPS were prepared as well, and a similar trend in their spatial distribution was observed (data not shown). Since the covalently-binding DPPS permeates extensively across the microstructure of **P5**, it can be surmised that excess hydroxyl groups exist throughout the monolithic structure, and can thus offer sites for subsequent functionalization. The presence of excess hydroxyl groups in the micropore domain can also account for the substantial non-permanent (swelling)

**ADVANCED
SCIENCE NEWS**

www.advancedsciencenews.com

**｛M｝acro-
molecular
Chemistry and Physics**

www.mcp-journal.de

Scheme 2. Surface functionalization and immobilization of [BMIM+][BF4−], containing a cationic Rh(I)-NHC complex,[41] onto the surface of a hydroxyl-containing polyurethane-based monolith.
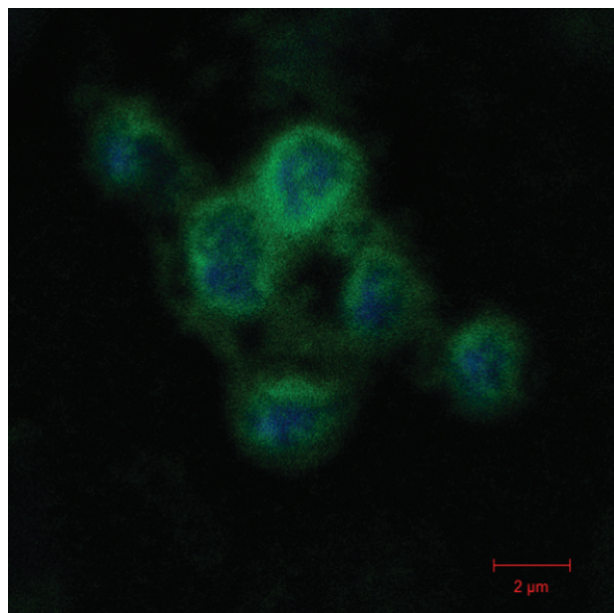

Figure 2. CLSM image of monolith **P5** first filled with rhodamine B—PEG (green), then functionalized with DPPS (blue).

porosity observed due to the swelling of the monolith structure in "good" polymer solvents such as $CHCl_3$ (vide supra).

2.6. Continuous Hydrosilylation of Alkynes Using Surface-Functionalized Poly(urethane)-Derived Monolith-Supported ILs

The hydrosilylation of both aromatic and aliphatic 1-alkynes, that is, phenylacetylene, 4-ethynyltoluene, 4-ethynylanisole, 1-hexyne, 1-octyne, and 1-nonyne, with $HSiMe_2Ph$ was performed under continuous biphasic conditions at 55 °C using [BMIM+][BF4−] as monolith-supported IL phase, methyl tert-butyl ether (MTBE) as the second liquid transport phase and the cationic Rh-NHC complex [1-(pyrid-2-yl)-3-mesityl)-imidazol-2-ylidene))(η^4-1,5-cyclooctadiene)Rh(I) tetrafluoroborate][41] dissolved in the IL phase, applying a linear flow of 0.2 mL·min−1. In general, the choice of the IL is a crucial factor in IL-supported biphasic catalysis.[22] Thus, the BF_4^- anion was chosen to prevent anion metathesis with the catalyst and to ensure immiscibility with the second transport phase, that is, with MTBE.

For comparison, hydrosilylation reactions were also carried out at 55 °C under biphasic conditions using 1 mol-% of the cationic Rh(I) NHC complex with respect to the 1-alkyne dissolved in [BMIM+][BF4−], employing MTBE as secondary liquid phase. Reactions were monitored by ¹H nuclear magnetic resonance (NMR) and gas-chromatography-mass spectroscopy

Table 2. Hydrosilylation of terminal alkynes.

Substrate	Biphasic conditions[a]			Continuous conditions[b]		
	$\beta(Z)/\beta(E)/\alpha$	Z/E	Conversion [%]	$\beta(Z)/\beta(E)/\alpha$	Z/E	Conversion [%]
Phenylacetylene	2/80/18	0.02	45	40/30/30	1.33	34
4-Ethynyltoluene	1/85/14	0.01	67	35/45/20	0.78	39
4-Ethynylanisole	-/75/25	0	78	62/19/19	3.26	24
1-Hexyne	20/55/25	0.36	45	35/42/23	0.83	24
1-Octyne	6/75/19	0.08	29	59/22/19	2.68	12
1-Nonyne	7/73/20	0.09	42	52/30/18	1.73	19

[a] 1 mol% Rh-catalyst, [BMIM$^+$][BF$_4$$^-$]:MTBE = 1:5, 55 °C, 12 h; [b] Rh@[BMIM][BF$_4$] immobilized on surface grafted monolith **P5**, MTBE, 55 °C, 0.2 mL·min^{-1}, 24–48 h, catalyst loading 8 mg/monolith.
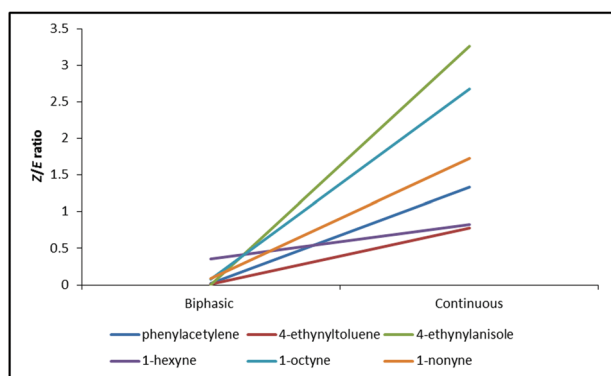

Figure 3. Z/E ratio under biphasic and continuous conditions.

(GC-MS) using *n*-dodecane as internal standard. With all substrates, a clear preference for the thermodynamically more stable $\beta(E)$-isomer in the range of 55–85% was observed under biphasic conditions (**Table 2** and **Figure 3**). Conversions between ≈20% and 80% were chosen to prevent any post-reaction isomerization. As can be seen from Figure 3, the Z/E ratio (Z-content) of the hydrosilylation products increased substantially up to 3.26 for 4-ethynylanisole (62% Z-isomer) in case the reactions were performed under monolith-supported, biphasic continuous flow conditions compared to reactions carried out under biphasic conditions. This increase in Z-selectivity can be attributed to a confinement effect[41] created by the constrained geometry inside the small mesopores, which affects the transition state of the Rh-catalyst, favoring a Z-arrangement (**Figure 4**).

In line with that are the lower conversions with the monolith-supported catalyst, which are a consequence of the slower diffusion inside the pores. Notably, the monitoring of the hydrosilylation of 4-ethynyltoluene and 1-octyne, respectively, with dimethylphenylsilane under biphasic conditions revealed the formation of the $\beta(E)$-isomer from the beginning of the reaction, ruling out any possible Z → E isomerization (Figure S28, Supporting Information).
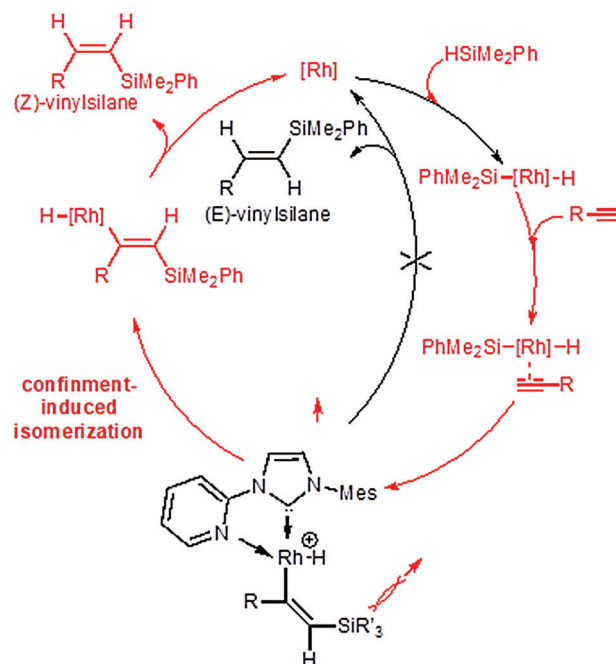

Figure 4. Confinement induced formation of Z-isomers. The preferred reaction pathway is shown in red.

3. Conclusion

In summary, non-porous polyurethane-based monoliths were prepared. The rigid non-porous structure enabled for high linear flow rates up to 13 mm/min with low counter pressure (< 7 bar). The pore size distribution obtained from ISEC confirms the non-porous nature of the monoliths but reveals some solvent-induced swelling propensity. The first polyurethane-based monolith with tailored mesoporosity in the range of ≈2–10 nm were synthesized via SIPS by carefully changing the ratio of the porogenic solvents. Surface-functionalization of the poly(urethane)-derived monoliths was accomplished

**ADVANCED
SCIENCE NEWS**

www.advancedsciencenews.com

**Macro-
molecular
Chemistry and Physics**

www.mcp-journal.de

via reaction with 4-isocyanatophenyltrimethylammonium tetrafluoroborate. Immobilization of the IL [BMIM$^+$][BF$_4^-$] containing [1-(pyrid-2-yl)-3-mesityl)-imidazol-2-ylidene))(η^4-1,5-cyclooctadiene)rhodium(I) tetrafluoroborate] on a mesoporous monolith allowed for for hydrosilylation reactions under continuous polymer-supported biphasic conditions. Notably, the selectivity toward β-(Z)-vinylsilanes increased using the Rh(I) catalyst supported on surface-modified monoliths under continuous flow, which can be attributed to a steric confinement effect created by the mesoporous system.

4. Experimental Section

General: Triethylene glycol (TEG, 99%), 1,1,1-tris(hydroxymethyl) propane (THP, 98%), 1,4-dioxane (99.8%), 4,4′-methylenebis(phenyl isocyanate) (98%) were purchased from Sigma-Aldrich. Dibutyltin dilaurate (DBTDL, 95%), polyethylene glycol (PEG$_{300}$), diglyme (99.0%) were purchased from Tokyo Chemical Industry (TCI). Hexamethylene-1,6-diisocyanate trimer (HMDI) was supplied by Covestro AG.

The total porosity, the pore volume, and the pore size distribution were determined by ISEC.[38,39] For these purposes, the retention times of toluene and of narrow polystyrene (PS) standards (D ≤ 1.02) with 162 ≤ M_n ≤ 2 000 000 g mol^{-1} were measured in CHCl$_3$ at 35 °C applying a flow rate of 2 mL min^{-1}. N$_2$-sorption analyses were conducted at 77 K on a Quantachrome Autosorb iQ MP automatic volumetric instrument. Polyurethane monoliths were degassed for 20 h at 25 °C under vacuum prior to the gas adsorption studies. Surface areas were evaluated using the Brunauer–Emmett–Teller model applied between p/p_0 ratios of 2.4 10^{-2} and 0.9. Pore size distributions were calculated using the slit pore, non-local density functional theory equilibrium model. Electron microscopy measurements were carried out on a Zeiss Auriga field-emission scanning electron microscope. An accelerating voltage of 2.50 kV was used for high resolution. Pt/Pd (80/20) sputtering was used for sample preparation. Infrared (IR) spectra were recorded on a Bruker IFS 28 using ATR technology in NaCl cuvettes or as KBr pellets. NMR spectra were recorded on a Bruker Avance III 400 spectrometer or a Bruker DRX 250 spectrometer in the indicated solvent at 25 °C; data were listed in parts per million downfield from tetramethylsilane as internal standard. GC-MS data were obtained on an Agilent Technologies 5975C inert MSD equipped with a triple-axis detector, a 7693 autosampler, and a 7890A GC system using an SPB-5 fused silica column (34.13 m × 0.25 mm × 0.25 µm film thickness). The injection temperature was set to 150 °C. The column temperature ramped from 45 to 250 °C within 8 min, and was then held for further 5 min. The column flow was 1.05 mL min^{-1}.

Synthesis of Non-Porous Monoliths: The typical synthetic procedure used was as follows: stainless steel columns (8 × 300 mm) were cleaned, rinsed, and sonicated in a 1:1 mixture of CHCl$_3$ and acetone. Finally, they were dried for 3 h at 120 °C. A stainless steel column (8 × 30 mm) was attached on top of a second stainless steel column that was closed on the lower end as an extension to compensate for the longitudinal volume shrinkage and was again removed after monolith synthesis. For nonporous polyurethanes, solution I consisted of PEG$_{300}$, THP, MTBE, and DBTDL, all dissolved in dioxane. Solution II contained MDI dissolved in dioxane. Both solutions were combined and thoroughly mixed. Then, the solution was filled into the vertically oriented steel columns and polymerization was allowed to proceed for 18 h at 45 °C. For polyurethane monoliths with tailored mesoporosity, solution I consisted of TEG, THP, MTBE, and DBTDL, all dissolved in dioxane. Solution II consisted of MDI dissolved in dioxane. Both solutions were combined and thoroughly mixed. Then, the solution was filled into the vertically oriented steel columns and polymerization was allowed to proceed for 18 h at 45 °C. Once polymerizations were complete, all columns were flushed with CHCl$_3$ at a flow of 0.1 mL·min^{-1} for 2 h.

Synthesis of [NCO-C$_6$H$_4$-NMe$_3^+$][BF$_4^-$]: 4-(Dimethylamino)phenyl isocyanate (0.2 g, 1.2 mmol) and methyl iodide (1 g, 7 mmol) were stirred for 3 h at 50 °C. The product was purified by washing with diethyl ether, then dried in vacuo. AgBF$_4$ (0.7 mmol) was then added to [NCO-C$_6$H$_4$-NMe$_3^+$][I$^-$] (1.2 mmol) in CH$_2$Cl$_2$ at room temperature. The reaction mixture was stirred for 1 h, then the yellow precipitate of AgI was filtered off and the product was purified by washing with diethyl ether and dried in vacuo. FT-IR (cm^{-1}): 2280 (s, NCO), 1736 (bs), 1041 (s), 722 (s), 568 (s); ^{1}H-NMR (CDCl$_3$): δ 8.0 (d, 2 H, J = 8 Hz), 7.33 (d, 2 H, J = 8 Hz), 4.06 (s, 9 H); ^{19}F-NMR (CDCl$_3$) δ 148.2; ^{13}C NMR (CDCl$_3$): δ 144.9, 135.0, 126.7, 125.1, 122.5, 27.0. HRMS calculated for C$_{10}$H$_{13}$N$_2$O: 177.1022, found: 177.1021.

Surface-Grafting of Poly(urethane)-Derived Monolithic Supports: For the grafting of [NCO-C$_6$H$_4$-NMe$_3^+$][BF$_4^-$] to the −OH functionalized monoliths, the column was flushed with CH$_2$Cl$_2$ for 2 h at a flow rate of 0.1 mL·min^{-1}. The ionic monomer (5 mg, one equiv. with respect to the excess hydroxyl groups) was dissolved in a 1:10 mixture of DMF and CH$_2$Cl$_2$ in the presence of DBTDL (11 mg). This mixture was injected into the monolith using a syringe pump at a flow rate of 0.03 mL·min^{-1}. The ionic monomer-loaded monolith was then sealed and kept at 45 °C for 12 h. To remove the DBTDL and excess [NCO-C$_6$H$_4$-NMe$_3^+$][BF$_4^-$], the column was flushed with CH$_2$Cl$_2$ for 2 h at a flow rate of 0.1 mL·min^{-1}.

CLSM Experiments: CLSM experiments were performed on an LSM-880 confocal microscope (Carl Zeiss, Jena, Germany). The fluorescence of DPPS was excited at 405 nm using a diode laser (LDH-D-C-405, PicoQuant, Berlin, Germany). The fluorescence of RhB-PEG was excited at 543 nm using a HeNe laser. The laser beams were focused onto the studied samples through an Alpha-Plan-Apochromat 100×/1.46 oil-immersion objective (Carl Zeiss, Jena, Germany). The same objective was used to record the emission. The emitted fluorescence was directed through a confocal pinhole (set to 1 Airy unit) and detected by a spectral detection unit (Quasar, Carl Zeiss, Jena, Germany).

Immobilization of [BMIM$^+$][BF$_4^-$] Containing the Ionic Rh-Catalyst on the Surface of the Monoliths: The cationic Rh-NHC catalyst (8 mg) and [BMIM$^+$][BF$_4^-$] (100 mg) were dissolved in CH$_2$Cl$_2$. The solution was then introduced into the monolith. Vacuum was applied for 3 h to remove all solvents. Prior to use, the support was flushed with heptane overnight applying a flow rate of 0.1 mL·min^{-1}.

Typical Procedure for the Rh-Catalyzed Hydrosilylation of Alkynes Under Biphasic Conditions: The cationic Rh complex (1 mol% with respect to the 1-alkyne) was dissolved in [BMIM][BF$_4$] (50 mg) and MTBE (0.5 mL) was added. The alkyne (1 equiv.) and dimethylphenylsilane (1.5 equiv.) were then added to the reaction mixture along with 10 µL of the internal standard (dodecane) and the biphasic mixture was then vigorously stirred for 12 h. Conversion was determined by GC-MS analysis while the Z/E ratios were determined by NMR.

Typical Procedure for the Rh-Catalyzed Hydrosilylation of Alkynes Under Continuous Flow: Hydrosilylation reactions were performed using the 1-alkyne (140 µL 1.0 equiv) and dimethylphenylsilane (280 µL, 1.5 equiv.) as the coupling partners in the presence of MTBE. An HPLC column (4.6 mm × 150 mm, V_{column} = 2.49 mL) containing the monolith loaded with [BMIM$^+$][BF$_4^-$] with the ionic Rh-catalyst (8 mg) dissolved therein was used. Dodecane (10 µL) was used as internal standard. The HPLC monolith column was placed inside an oven and the reaction mixture was pumped through the monolith column at 55 °C for 48–60 h at a flow rate of 0.2 mL·min^{-1}.

*Filling of Monolith **P5** with Rhodamine B-PEG, Followed by Functionalization with DPPS*: 4 mg of rhodamine B-PEG and 0.8 g of PEG were dissolved in 12 mL H$_2$O. Upon homogenization, 0.1 g of the **P5** was added and the mixture was stirred at room temperature for 24 h. The rhodamine B-PEG-filled monolith was separated by filtration and dried in vacuo at 80 °C for 24 h. 50 mg of the RhB-PEG filled monolith were treated with 1.015 mL of DPPS and reaction was allowed to proceed under solventless conditions for 1 h at room temperature. All unreacted DPPS was washed off with *n*-hexane (30 mL) and the sample was allowed to dry under air at room temperature.

Typical Procedure for the Preparation of Monolith Dispersions for CLSM: 15 mg of the monolith were dispersed in 5 mL of 2-propanol and then sonicated for 45 min. The dispersion was vortexed and 100 µL of the dispersion was drop cast on plasma-cleaned 25 mm round microscope glass slides.

Supporting Information

Acknowledgements

Conflict of Interest

The authors declare no conflict of interest.

Data Availability Statement

The data that support the findings of this study are available from the corresponding author upon reasonable request.

Keywords

[1] F. Švec, C. G. Huber, *Anal. Chem.* **2006**, *78*, 2100.
[2] F. Švec, L. Geiser, *LCGC North Am.* **2006**, *24*, 22.
[3] F. Švec, T. B. Tennikova, Z. Deyl, in *Monolithic Materials: Preparation, Properties and Application*, Journal of Chromatography Library, *Vol. 67*, Elsevier, Amsterdam **2003**.
[4] B. Mayr, G. Hölzl, K. Eder, M. R. Buchmeiser, C. G. Huber, *Anal. Chem.* **2002**, *74*, 6080.
[5] B. Mayr, R. Tessadri, E. Post, M. R. Buchmeiser, *Anal. Chem.* **2001**, *73*, 4071.
[6] E. F. Hilder, F. Švec, J. M. J. Fréchet, *Anal. Chem.* **2004**, *76*, 3887.
[7] A. E. Rodrigues, Z. P. Lu, J. M. Loureiro, G. Carta, *J. Chromatogr. A* **1993**, *653*, 189.
[8] A. E. Rodrigues, A. M. D. Ramos, J. M. Loureiro, M. Diaz, Z. P. Lu, *Chem. Eng. Sci.* **1992**, *47*, 4405.
[9] A.-R. E. Rodrigues, J. C. Lopes, Z. P. Lu, J. M. Loureiro, M. M. Dias, *J. Chromatogr.* **1992**, *590*, 93.
[10] A. E. Rodrigues, L. Zuping, J. M. Loureiro, *Chem. Eng. Sci.* **1991**, *46*, 2765.
[11] A. E. Rodrigues, B. J. Ahn, A. Zoulalian, *AIChE J.* **1982**, *28*, 541.
[12] E. B. Anderson, M. R. Buchmeiser, *ChemCatChem* **2012**, *4*, 30.
[13] M. R. Buchmeiser, *Macromol. Rapid. Commun.* **2001**, *22*, 1081.
[14] M. R. Buchmeiser, *Polymer* **2007**, *48*, 2187.
[15] R. Bandari, W. Knolle, A. Prager-Duschke, M. R. Buchmeiser, *Macromol. Rapid Commun.* **2007**, *28*, 2090.
[16] M. J. Beier, W. Knolle, A. Prager-Duschke, M. R. Buchmeiser, *Macromol. Rapid Commun.* **2008**, *29*, 904.
[17] S. Xie, F. Švec, J. M. J. Fréchet, *Polym. Prepr. (Am. Chem. Soc., Div. Polym. Chem.)* **1997**, *38*, 211.
[18] S. Xie, F. Švec, J. M. J. Fréchet, *Biotechnol. Bioeng.* **1999**, *62*, 30.
[19] B. Autenrieth, W. Frey, M. R. Buchmeiser, *Chem. - Eur. J.* **2012**, *18*, 14069.
[20] L. C. Hansen, R. E. Sievers, *J. Chromatogr.* **1974**, *99*, 123.
[21] C. Lee, B. Sandig, M. R. Buchmeiser, M. Haumann, *Catal. Sci. Technol.* **2018**, *8*, 2460.
[22] B. Sandig, M. R. Buchmeiser, *ChemSusChem* **2016**, *9*, 2917.
[23] B. Sandig, L. Michalek, S. Vlahovic, M. Antonovici, B. Hauer, M. R. Buchmeiser, *Chem. - Eur. J.* **2015**, *21*, 15835.
[24] M. R. Buchmeiser, *ChemCatChem* **2021**, *13*, 785.
[25] S. T. Emmerling, F. Ziegler, F. R. Fischer, R. Schoch, M. Bauer, B. Plietker, M. R. Buchmeiser, B. V. Lotsch, *Chem. - Eur. J.* **2022**, *28*, e202104108.
[26] P. K. R. Panyam, B. Atwi, F. Ziegler, W. Frey, M. Nowakowski, M. Bauer, M. R. Buchmeiser, *Chem. - Eur. J.* **2021**, *27*, 17220.
[27] U. Tallarek, J. Hochstrasser, F. Ziegler, X. Huang, C. Kübel, M. R. Buchmeiser, *ChemCatChem* **2021**, *13*, 281.
[28] F. Ziegler, H. Kraus, M. J. Benedikter, D. Wang, J. R. Bruckner, M. Nowakowski, K. Weißer, H. Solodenko, G. Schmitz, M. Bauer, N. Hansen, M. R. Buchmeiser, *ACS Catal.* **2021**, *11*, 11570.
[29] F. Ziegler, T. Roider, M. Pyschik, C. P. Haas, D. Wang, U. Tallarek, M. R. Buchmeiser, *ChemCatChem* **2021**, *13*, 2234.
[30] F. Ziegler, J. Teske, I. Elser, M. Dyballa, W. Frey, H. Kraus, N. Hansen, J. Rybka, U. Tallarek, M. R. Buchmeiser, *J. Am. Chem. Soc.* **2019**, *141*, 19014.
[31] S. H. A. M. Leenders, R. Gramage-Doria, B. De Bruin, J. N. H. Reek, *Chem. Soc. Rev.* **2015**, *44*, 433.
[32] S. A. Miners, G. A. Rance, A. N. Khlobystov, *Chem. Soc. Rev.* **2016**, *45*, 4727.
[33] S. Zhang, J. Zhang, Y. Zhang, Y. Deng, *Chem. Rev.* **2017**, *117*, 6755.
[34] F. Švec, *LC-GC: LC Column Technol. Suppl.* **2004**, *June*, 18.
[35] F. Švec, *J. Sep. Sci.* **2004**, *27*, 17.
[36] F. Svec, *J. Sep. Sci.* **2004**, *27*, 1419.
[37] F. Švec, *LC-GC Europe* **2005**, *18*, 17.
[38] I. Halász, K. Martin, *Angew. Chem.* **1978**, *90*, 954; *Angew. Chem., Int. Ed.* **1978**, *17*, 901.
[39] I. Halász, K. Martin, *Ber. Bunsenges. Phys. Chem.* **1975**, *79*, 731.
[40] H. Acikalin, F. Ziegler, D. Wang, M. R. Buchmeiser, *Macromol. Chem. Phys.* **2021**, *222*, 2100247.
[41] P. K. R. Panyam, B. Atwi, F. Ziegler, W. Frey, M. Nowakowski, M. Bauer, M. R. Buchmeiser, *Chem. - Eur. J.* **2021**, *27*, 17220.